Effect of Carboxyl-Terminal Truncation on Structure and Lipid Interaction of Human Apolipoprotein E4[†]

Masafumi Tanaka,[‡] Charulatha Vedhachalam,[§] Takaaki Sakamoto,[‡] Padmaja Dhanasekaran,[§] Michael C. Phillips,[§] Sissel Lund-Katz,*[,§] and Hiroyuki Saito[‡]

Department of Biophysical Chemistry, Kobe Pharmaceutical University, Kobe 658-8558, Japan, and Lipid Research Group, The Children's Hospital of Philadelphia, University of Pennsylvania School of Medicine, Philadelphia, Pennsylvania 19104-4318

Received January 5, 2006; Revised Manuscript Received February 13, 2006

ABSTRACT: Apolipoprotein (apo) E4 has been identified as a major risk factor for Alzheimer's disease. Recently, apoE4 was found to undergo proteolytic cleavage in Alzheimer's disease brains, resulting in neurotoxic C-terminal-truncated fragments. In this study, we examined the effect of progressive truncation of the C-terminal domain in apoE4 on its lipid-free structure and lipid binding properties. Circular dichroism measurements demonstrated that deletion of residues 273−299 or 261−299 significantly decreased the number of helical residues, suggesting that the C-terminal residues 261−299 have α-helical structure. Although the progressive deletions in the C-terminal domain appear to somewhat increase thermal stability, apoE4 (Δ273−299) and apoE4 (Δ261−299) showed stability similar to that of the apoE4 22-kDa fragment (residues 1−191) when denatured with guanidine-HCl, indicating that residues 192−272 have a negligible effect on the stability of the C-terminal-truncated apoE4. Comparison of Trp-264 fluorescence in single Trp mutants of full-length and C-terminal-truncated apoE4 (Δ273−299) indicated that the C-terminal domain structure in the latter is both less organized and cooperative. In addition, comparison of the binding of the C-terminal-truncated mutants to a hydrophobic fluorescent dye and to lipid emulsions revealed that residues 261−272 create a hydrophobic site which is critical for lipid binding. These results suggest that removal of a hydrophobic C-terminal α-helical segment (residues 273−299) to create C-terminal-truncated apoE4 forms found in brain leads to less organized C-terminal structure while still retaining a second α-helical lipid-binding region (residues 261−272) that is available for interaction with cell membranes and other proteins such as amyloid β peptide.

Apolipoprotein E (apoE) is a key protein regulating lipid transport in the cardiovascular and central nervous systems (*1*−*4*). In humans, apoE exists in three major isoforms, apoE2, apoE3, and apoE4, each differing by cysteine and arginine at positions 112 and 158 (*2*). ApoE3, the most common form, contains cysteine and arginine at these positions, respectively, whereas apoE2 contains cysteine and apoE4 contains arginine at both sites. ApoE4 is known to be a major risk factor for coronary heart disease and Alzheimer's disease (AD[1]) (*5*−*7*). ApoE4 is found in neurofibrillary tangles and amyloid plaques, which are neuropathological hallmarks of AD (*8*−*10*). ApoE4 is also associated with neuronal damage, including poor outcome and recovery after neurological injury (*11*) and other central nervous system stresses (*12*).

ApoE contains two independently folded functional domains, a 22-kDa N-terminal domain (residues 1−191) and a 10-kDa C-terminal domain (residues 222−299) (*2*, *13*). The N-terminal domain is folded into a four-helix bundle of amphipathic α-helices and contains the receptor binding region (around residues 136−150 in helix 4) (*14*, *15*). The C-terminal domain also contains amphipathic α-helices that are involved in binding to lipoprotein particles (*16*−*18*) and in self-association (*16*, *19*, *20*). In apoE4, these two domains interact in a manner that differs from the situation in the other isoforms; Arg-112 causes a rearrangement of the Arg-61 side chain in the N-terminal domain of apoE4, allowing it to interact with Glu-255 in the C-terminal domain (*21*, *22*). Indeed, fluorescence resonance energy transfer studies demonstrated a closer spatial proximity of the two domains in apoE4 compared to apoE3 (*23*, *24*) This domain interaction is responsible for the less organized structure of the C-terminal domain in apoE4 (*25*) and contributes to preferential association of apoE4 with very low-density lipoproteins (*21*, *22*). The domain interaction in apoE4 was also shown to occur in living neuronal cells (*26*) and in vivo in knock-in mice, in which domain interaction was introduced into mouse apoE by mutating Thr-61 to Arg (*27*). Although domain interaction has been suggested to contribute to the association of apoE4 with atherosclerosis and neurodegen-

[†] This work was supported by NIH Grant HL56083 and the Mochida Memorial Foundation for Medical and Pharmaceutical Research.

* To whom correspondence should be addressed. Mailing address: The Children's Hospital of Philadelphia, Abramson Research Building, Suite 1102, 3615 Civic Center Blvd., Philadelphia, PA 19104-4318. Tel: (215) 590-0588. Fax: (215) 590-0583. E-mail: katzs@email.chop.edu.

[‡] Kobe Pharmaceutical University.

[§] University of Pennsylvania School of Medicine.

[1] Abbreviations: Aβ, amyloid β; AD, Alzheimer's disease; ANS, 8-anilino-1-naphthalenesulfonic acid; apoE, apolipoprotein E; CD, circular dichroism; GdnHCl, guanidine hydrochloride.

10.1021/bi060023b CCC: $33.50
Published on Web 03/10/2006

eration (*13*, *22*, *26*), the underlying mechanisms remain unknown to date.

Recently, apoE was found to undergo proteolytic cleavage in AD brains, resulting in cytotoxic C-terminal-truncated fragments (*28*). This proteolysis occurs in neurons but not in astrocytes, with more fragments being generated from apoE4 than from apoE3 (*28*, *29*). These fragments, especially apoE4 (Δ272−299), can cause neurodegeneration and induce neurofibrillary tangle-like inclusions in cultured neuronal cells as well as in transgenic mice (*28*, *30*), suggesting that intraneuronal proteolytic processing of apoE could trigger apoE4-related neuropathology and promote the development of AD. Interestingly, the presence of a lipid-binding region of apoE (residues 244−272) appears to be critical for apoE fragments to have neurotoxic effects in vivo (*8*, *30*), although this region alone is insufficient for neurotoxicity (*31*).

To understand the molecular basis for the role of the C-terminal domain in the structure and function of apoE4, we examined the effect of progressive truncation of the C-terminal domain (Δ273−299 and Δ261−299) in apoE4 on its lipid-free structure and state of self-association. Although both mutants lack the C-terminal α-helical segment (residues 268−289) that is responsible for self-association of apoE, Δ273−299 contains residues 244−272 that are critical for lipoprotein binding (*16*). In addition, we compared the lipid binding ability of these C-terminal-truncated mutants with full-length apoE4 using lipoprotein-like emulsion particles. The results show that the removal of residues 273−299 from apoE4 leads to less ordered organization in the C-terminal domain, with residues 261−272 being available for hydrophobic interactions such as lipid binding.

EXPERIMENTAL PROCEDURES

Materials. Egg yolk phosphatidylcholine and triolein were purchased from Sigma (St. Louis, MO), and stock solutions were stored in chloroform/methanol (2/1) under nitrogen at −20 °C. [^{14}C]Formaldehyde (40−60 Ci/mol) in distilled water was purchased from Perkin Elmer Life Sciences (Boston, MA). 8-Anilino-1-naphthalenesulfonic acid (ANS) was purchased from Molecular Probes (Eugene, OR). Ultrapure guanidine hydrochloride (GdnHCl) was from ICN Pharmaceuticals (Costa Mesa, CA).

Expression and Purification of Proteins. The full-length human apoE4 and its 22-kDa, 12-kDa (residues 192−299), and 10-kDa fragments were expressed and purified as described (*18*, *25*). The mutations in apo E4 to create the truncated forms (Δ261−299 and Δ273−299) were made using PCR methods, and the single tryptophan point mutations (W@264) were made using the QuikChange site-directed mutagenesis kit (Stratagene, La Jolla, CA). The cDNA was ligated into a thioredoxin fusion expression vector pET32a (+) (Novagen, Madison, WI) and transformed into the *Escherichia coli* strain BL21 star (DE3) (Invitrogen, Carlsbad, CA). The resulting thioredoxin-apoE fusion proteins were expressed and purified as described (*18*). The expression and yields of the truncated Δ261−299 and Δ273−299 variants were similar to those of the full-length apo E4 protein. The apoE preparations were at least 95% pure as assessed by SDS−PAGE. In all experiments, the apoE sample was freshly dialyzed from 6 M GdnHCl solution into buffer solution before use.

Circular Dichroism (CD) Spectroscopy. Far-UV CD spectra were recorded from 185 to 260 nm at 25 °C using a Jasco J-600 or Aviv 62DS spectropolarimeter. After dialysis, the apoE sample was diluted to 25−50 μg/mL in 10 mM phosphate buffer (pH 7.4) for obtaining the CD spectrum. The results were corrected by subtracting the buffer baseline or a blank sample containing an identical concentration of GdnHCl. The α-helix content was derived from the molar ellipticity at 222 nm, $[\theta]_{222}$, according to the following equation (*32*, *33*):

$$\% \text{ α-helix} = ([\theta]_{222} + 3000)/(36000 + 3000) \times 100$$

The thermal denaturation was monitored from the change in molar ellipticity at 222 nm over the temperature range 20−90 °C, as described (*33*). The cooperativity index, *n*, describing the sigmoidicity of the thermal denaturation curve was calculated by applying the Hill equation, $n = (\log 81)/\log(T_{0.9}/T_{0.1})$, where $T_{0.1}$ and $T_{0.9}$ are the temperatures where the fractional completions of the unfolding transition are 0.1 and 0.9, respectively. The equilibrium constants of denaturation, K_D, at each temperature were derived from the measured molar ellipticity at each temperature and the molar ellipticities of the native and denatured forms of the protein, as described (*34*). The van't Hoff enthalpy, ΔH_v, was calculated from the slope of the line fitted by linear regression to the equation, $\ln K_D = -(\Delta H_v/R)(1/T) + \text{constant}$, where *R* is the gas constant and *T* is temperature. For monitoring chemical denaturation, proteins at concentration of 50 μg/mL were incubated overnight at 4 °C with GdnHCl at various concentrations. K_D values at given GdnHCl concentrations were calculated from the ellipticity values (*34*). The free energy of denaturation, $\Delta G_D°$, the midpoint of denaturation, $D_{1/2}$, and the *m* value, which reflects the cooperativity of denaturation in the transition region, were determined by the linear equation $\Delta G_D = \Delta G_D° - m[\text{GdnHCl}]$, where $\Delta G_D = -RT \ln K_D$.

Fluorescence Measurements. Fluorescence measurements were carried out with a Hitachi F-4500 fluorescence spectrophotometer at 25 °C in Tris buffer (10 mM Tris-HCl, 150 mM NaCl, 0.02% NaN_3, 1 mM EDTA, pH 7.4). For monitoring chemical denaturation, proteins at concentrations of 50−100 μg/mL were incubated overnight at 4 °C with GdnHCl at various concentrations. The emission spectra were recorded from 300 to 400 nm using a 295 nm excitation wavelength to avoid tyrosine fluorescence. K_D values at given GdnHCl concentrations were derived from the change in fluorescence intensity at 335 nm (*35*). $\Delta G_D°$, $D_{1/2}$, the *m* value, and the cooperative index were determined as described above. ANS fluorescence spectra were collected from 400 to 600 nm at an excitation wavelength of 395 nm in the presence of 50 μg/mL protein and an excess of ANS (250 μM) (*36*).

Gel Filtration Chromatography. The various apoE preparations were trace-labeled with ^{14}C to a specific activity of ∼1 μCi/mg protein by reductive methylation of lysines with [^{14}C]formaldehyde (*18*, *37*, *38*). Typically, apoE samples at a concentration of 5−50 μg/mL were subjected to gel filtration on a calibrated Superdex 200 column (60 × 1.6 cm) using an Akta FPLC system, and eluted with Tris buffer at a flow rate of 1 mL/min (*39*). Two-milliliter fractions were collected, and radioactivity was determined by liquid scintil-

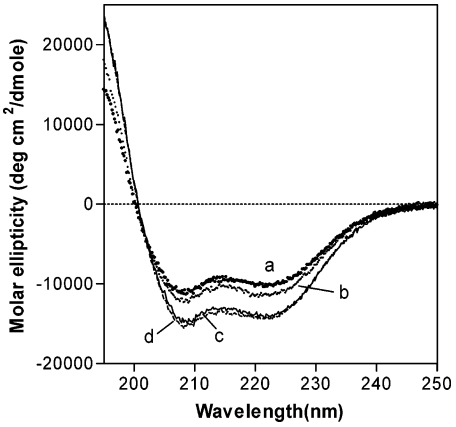

FIGURE 1: Far-UV CD spectra of apoE4 C-terminal-truncated mutants: apoE4 (Δ261−299) (a), apoE4 (Δ273−299) (b), apoE4 (c), and apoE4 22-kDa (d). Protein concentration was 50 μg/mL.

Table 1: α-Helix Content and Thermal Denaturation Parameters of ApoE4 C-Terminal Truncated Mutants

apoE4 variant	α-helix,[a] %	number of residues in α-helix	T_m,[b] °C	coopera-tivity index	ΔH_v,[c] kcal/mol
apoE4	44 ± 3	131	45	3.7	20
apoE4 (Δ273−299)	37 ± 2	102	45	5.4	26
apoE4 (Δ261−299)	35 ± 2	92	49	6.3	27
apoE4 22-kDa	46 ± 2	89	50	4.9	25

[a] Mean ± SD from at least three measurements. [b] The reproducibility in T_m is ± 1.5 °C. [c] Estimated error is ±2 kcal/mol.

lation counting. The elution volumes of the monomer and tetramer were established by using covalently cross-linked samples of apoE containing monomer and tetramers.

Binding of ApoE to Emulsion Particles. Triolein-egg phosphatidylcholine emulsion particles were prepared by sonication and purified by ultracentrifugation as described (*18*, *25*). The average particle diameter determined by quasi-elastic light scattering measurements was 120 ± 10 nm. The binding of apoE to emulsion particles at room temperature was assayed with a centrifugation method as described (*18*, *25*) using ^{14}C-labeled apoE samples. Binding data were fitted by nonlinear regression to a one binding site model with a GraphPad Prism program.

RESULTS

Secondary Structure and Thermal Unfolding of the C-Terminal-Truncated ApoE4. The secondary structure of the C-terminal-truncated apoE4 was analyzed by CD spectroscopy. Figure 1 shows the far-UV CD spectra of full-length, Δ273−299, Δ261−299, and 22-kDa (residues 1−191) apoE4. Although all spectra exhibited negative peaks at 208 and 222 nm, which are characteristic of an α-helical structure, significant reduction in molar ellipticities both at 208 and at 222 nm was observed for the C-terminal-truncated mutants. The α-helix contents estimated from the molar ellipticity at 222 nm are listed in Table 1. Compared with full-length apoE4, the decrease in the number of α-helical residues is consistent with the number of residues removed by truncation for both Δ273−299 and Δ261−299 mutants, indicating that residues 261−299 form α-helical structure in the lipid-free state (*40*, *41*). In contrast, the number of α-helical residues for the Δ261−299 mutant is comparable to that in the 22-kDa fragment, suggesting that residues 192−260 in apoE4 are largely nonhelical.

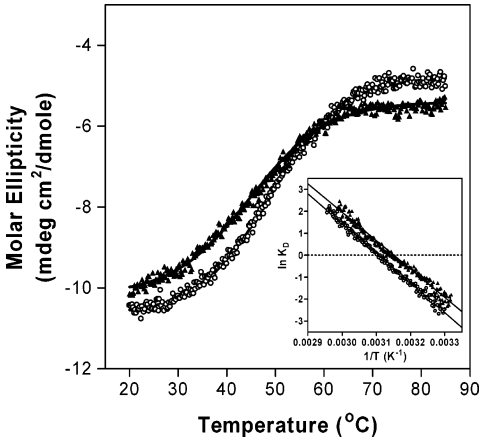

FIGURE 2: Thermal unfolding of apoE4 C-terminal-truncated mutants monitored by the ellipticity at 222 nm: apoE4 (Δ261−299) (○) and apoE4 (Δ273−299) (▲). The inset shows van't Hoff plots of ln K_D as a function of 1/T.

Figure 2 shows the thermal unfolding curves of Δ273−299 and Δ261−299 apoE4 monitored by the ellipticity at 222 nm. The shapes of the curves indicate the cooperative unfolding of Δ273−299 and Δ261−299 mutants. The midpoint temperature, T_m, the cooperativity index, and the van't Hoff enthalpy, ΔH_v, of thermal unfolding are summarized in Table 1. Progressive deletions in the C-terminal domain tend to increase the midpoint and cooperativity of unfolding, consistent with the concept of two structural domains in apoE, in which the N-terminal domain forms stable helix bundle structure whereas the C-terminal domain has less organized structure (*2*, *36*).

GdnHCl Denaturation of the C-Terminal-Truncated ApoE4. We next performed GdnHCl-induced denaturation experiments monitored by CD and Trp fluorescence. Since the C-terminal 10-kDa fragment of apoE has two Trp residues (Trp-264 and Trp-276), the tertiary structural change can be probed by monitoring Trp fluorescence spectra. Figure 3A shows far-UV CD spectra of the 10-kDa and 12-kDa fragments in the absence or presence of GdnHCl. The α-helix contents of the 10-kDa and the 12-kDa fragments were 50% and 49% (corresponding to 39 and 53 α-helical residues), respectively. Figure 3B shows Trp fluorescence spectra of the 10-kDa fragment at various GdnHCl concentrations. The fraction of the protein unfolded at a given GdnHCl concentration was derived from the changes in molar ellipticity at 222 nm or fluorescence emission intensity at 335 nm (*42*). As shown in Figure 3C, the denaturation curves of the 10-kDa fragment obtained from CD and Trp fluorescence measurements are superimposable, indicating a two-state unfolding transition (*35*). The midpoint of denaturation was 0.6 M GdnHCl, which is lower than previous results (*42*) probably because of a different self-aggregation state (*41*).

Figure 4 compares GdnHCl denaturation curves for full-length apoE4 and its 22-kDa and 10-kDa fragments. As seen for the 10-kDa fragment, CD and Trp fluorescence measurements gave similar denaturation curves for the 22-kDa fragment. The midpoint of denaturation for the 22-kDa fragment was 2.0−2.1 M GdnHCl, consistent with previous results (*42*). The denaturation of full-length apoE4 displayed a biphasic curve, in which the first and the second phases

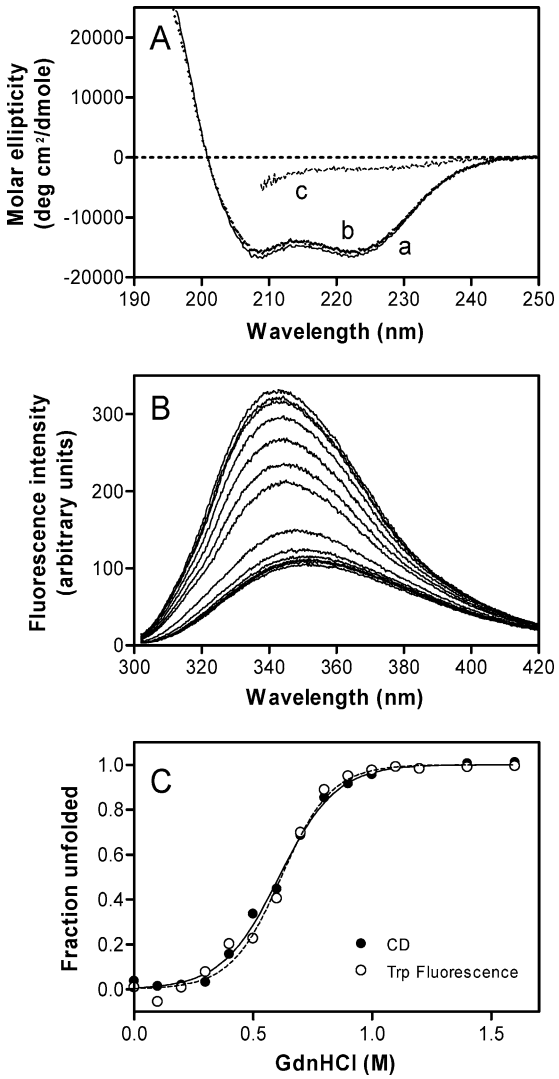

FIGURE 3: GdnHCl denaturation of apoE 10-kDa monitored by CD or Trp fluorescence. (A) Far-UV CD spectra of apoE 10-kDa (a) and 12-kDa (b) fragments. The data for the 10-kDa fragment in the presence of 1.6 M GdnHCl is also shown (c). Protein concentration was 50 μg/mL. (B) Fluorescence emission spectra of Trp in apoE 10-kDa (50 μg/mL) with changing GdnHCl concentration from 0 to 1.6 M. (C) Comparison of denaturation curves obtained from CD (●) or Trp fluorescence (○) measurements.

correspond to denaturation of the 10-kDa C-terminal and the 22-kDa N-terminal domains, respectively (*42*). The difference in the midpoints of the first phase (0.7 M for CD and 0.5 M for Trp fluorescence) may suggest the presence of an intermediate for unfolding of the C-terminal domain (*42*, *43*). In addition, the magnitude of the unfolded fraction corresponding to the C-terminal domain in the Trp fluorescence data (Figure 4B) is much larger than that in CD data (Figure 4A). This is because the former reflects the number of Trp residues located in the C-terminal domain whereas the latter reflects the number of amino acid residues in this domain. Figure 4 also shows GdnHCl denaturation of the C-terminal-truncated apoE4. The Δ273−299 and Δ261−299 mutants displayed identical denaturation curves to the 22-kDa fragment, indicating that residues 192−272 have a negligible effect on the structural stability of the C-terminal-truncated apoE4.

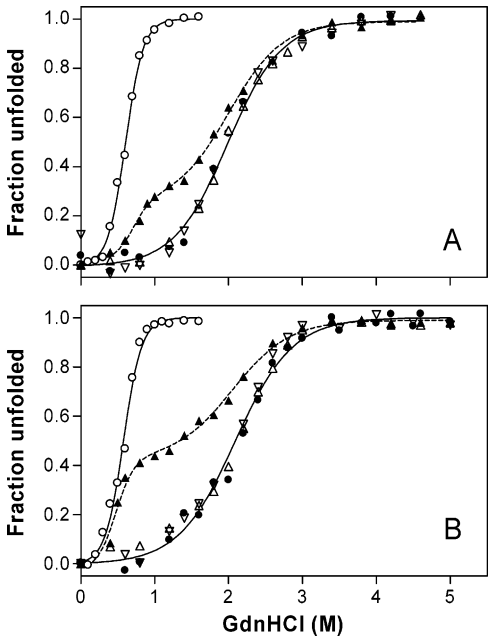

FIGURE 4: GdnHCl denaturation of full-length apoE4, 22-kDa and 10-kDa fragments of apoE4, and C-terminal-truncated apoE4 monitored by CD (A) and Trp fluorescence (B): full-length apoE4 (▲), apoE4 (Δ273−299) (●), apoE4 (Δ261−299) (▽), apoE4 22-kDa (△), and apoE 10-kDa (○).

GdnHCl Denaturation of ApoE4 Single Trp Mutants. To further examine the structural organization of the C-terminal domain in apoE4, single Trp mutants of apoE4 possessing a Trp residue at position 264 were subjected to GdnHCl denaturation. Out of 7 Trp residues in apoE4 (positions 20, 26, 34, and 39 in the N-terminal domain, 210 in the hinge region, and 264 and 276 in the C-terminal domain), 6 residues were mutated to Phe, leaving a single Trp at position 264 (apoE4 W@264) as a probe for the C-terminal domain (*44*). This mutation caused no change in structure and stability of the protein (data not shown). Figure 5A shows GdnHCl denaturation curves of the single Trp apoE4 monitored by the change in Trp fluorescence intensity. From the linear plots of the Gibbs free energy, ΔG_D, as a function of denaturant concentration (Figure 5B), the conformational stability, $\Delta G_D°$, the midpoint of denaturation, $D_{1/2}$, and the *m* value were derived (Table 2). Compared with the 10-kDa fragment, apoE4 W@264 displayed much less stability and cooperativity of unfolding, suggesting that the conformational stability of the C-terminal domain in apoE4 is much lower than that estimated from the isolated 10-kDa fragment. This does not appear to result from the presence of the hinge region (residues 192−215) because the 12-kDa fragment displayed stability and cooperativity similar to those of the 10-kDa fragment (Table 2). Comparison of apoE4 W@264 and apoE4 (Δ273−299) W@264 indicates that deletion of residues 273−299 significantly reduces the structural stability and cooperativity of the C-terminal domain in apoE4.

Gel Filtration Chromatography. ApoE is known to self-associate through the C-terminal domain in solution (*20*, *45*). To explore the effect of the C-terminal truncation on the self-association state of apoE4, gel filtration chromatography was employed (Figure 6). Full-length apoE4 eluted as a bimodal peak corresponding to the elution of both monomeric and tetrameric forms (*19*, *46*). In contrast, the 22-kDa fragment displayed a relatively sharp, single elution profile,

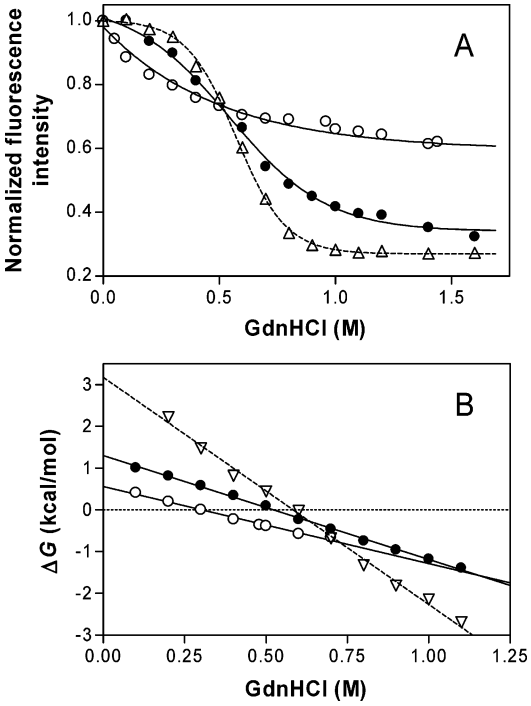

FIGURE 5: GdnHCl denaturation of single Trp mutants of apoE4 monitored by Trp fluorescence. Normalized fluorescence intensity at 335 nm (A) or Δ*G* (B) was plotted as a function of GdnHCl concentration; apoE4 W@264 (●) and apoE4 (Δ273−299) W@264 (○). ApoE 10-kDa (△ or ▽) was also shown for comparison.

Table 2: Thermodynamic Parameters of Denaturation of ApoE4 Single Trp Mutants

apoE4 variant	$\Delta G_D°$, kcal/mol	$D_{1/2}$, M	*m*	cooperativity index[a]
apoE4 W@264	1.3 ± 0.1	0.52 ± 0.02	2.5	2.8
apoE4 (Δ273−299) W@264	0.6 ± 0.1	0.31 ± 0.04	1.8	1.2
apoE 12-kDa	3.4 ± 0.2	0.65 ± 0.07	5.2	4.7
apoE 10-kDa	3.2 ± 0.2	0.58 ± 0.06	5.4	5.1

[a] Calculated as described under Experimental Procedures.

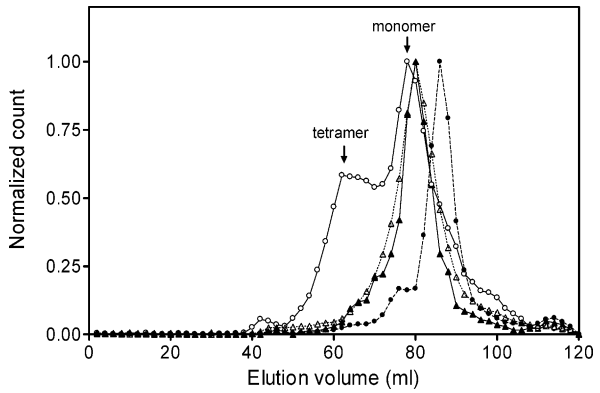

FIGURE 6: Elution profiles of gel filtration on a Superdex 200 column for apoE4 C-terminal-truncated mutants: full-length apoE4 (○), apoE4 (Δ273−299) (△), apoE4 (Δ261−299) (▲), and apoE4 22-kDa (●).

indicating the monomeric state (*45*, *46*). Although Δ273−299 displayed a slightly broader peak than that of Δ261−299, both mutants showed monomeric elution profiles, consistent with residues 273−299 being critical for tetramerization of apoE4 (*16*).

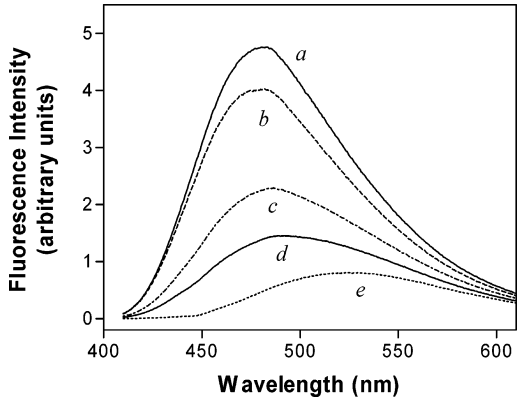

FIGURE 7: ANS fluorescence spectra in the presence of apoE4 C-terminal-truncated mutants: ApoE4 (a), apoE4 (Δ273−299) (b), apoE4 (Δ261−299) (c), apoE4 22-kDa (d), and free ANS (e).

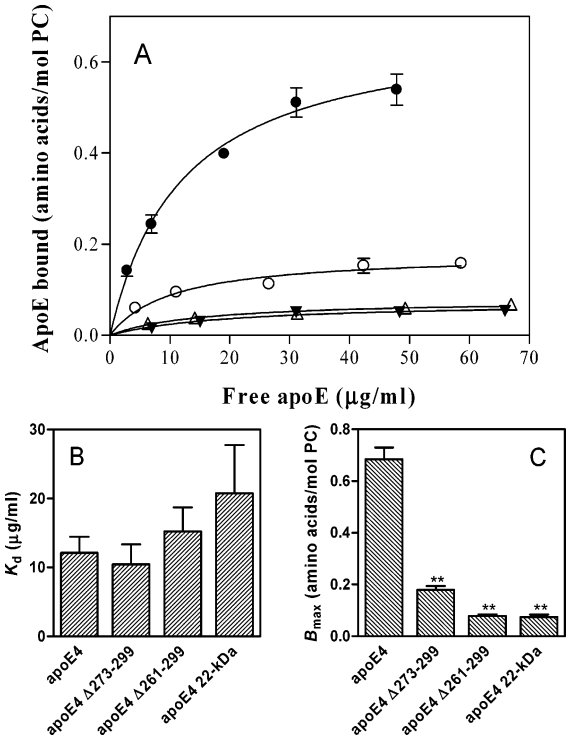

FIGURE 8: Binding of apoE4 C-terminal-truncated mutants to lipid emulsions. (A) Binding isotherms for apoE4 (●), apoE4 (Δ273−299) (○), apoE4 (Δ261−299) (△), and apoE4 22-kDa (▼). (B) Dissociation constant. (C) Maximal binding capacity. Binding parameters were derived from binding isotherms shown in Figure 8A. $^{**}p < 0.01$ compared to full-length apoE4.

ANS Binding. To explore the tertiary structure of the C-terminal-truncated apoE4, we monitored the binding of the hydrophobic fluorescent dye ANS (Figure 7). A significant increase in ANS fluorescence for full-length apoE4 predominantly comes from the hydrophobic sites created by the C-terminal domain (*25*) because the globular four-helix bundle structure in the N-terminal domain lacks exposed hydrophobic surface (*47*). Deletion of residues 273−299 caused a small decrease in ANS fluorescence, whereas a significant reduction was observed for the further deletion Δ261−299. This indicates that residues 261−272 create a significant exposed hydrophobic site in the C-terminal domain of apoE4.

Binding of the C-Terminal-Truncated ApoE4 to Lipid Emulsions. To compare the lipid-binding abilities of the

C-terminal-truncated apoE4 mutants, we used an emulsion binding assay (*18*, *25*). As shown in Figure 8, full-length apoE4 bound to the lipoprotein-like emulsion particles with high affinity and capacity (*18*). Deletion Δ273−299 caused a 4-fold reduction in maximal binding capacity without changing the binding affinity, indicating that residues 273−299 are critical for the binding of apoE4 to lipid (*16*, *21*, *48*). This decrease in the binding capacity also suggests that the Δ273−299 mutant binds to the emulsion surface with a conformation different from that of the full-length apoE4 (*18*). The deletion mutant Δ261−299 displayed a further reduction in binding capacity and bound similarly to the 22-kDa fragment. This suggests that residues 261−272 contribute to the lipid binding of apoE4 to some extent, whereas residues 192−260 are not involved in lipid binding.

DISCUSSION

ApoE is composed of two structural domains in which the 22-kDa N-terminal and the 10-kDa C-terminal domains are linked by a hinge region (*2*, *13*, *15*). The high-resolution structure of the N-terminal domain of apoE isoforms has been defined as a globular four-helix bundle organization (*14*, *21*, *49*). In contrast, the structural organization of the C-terminal domain is poorly understood. Computer-based secondary structure prediction identified three α-helical segments in the C-terminal domain (residues 203−223, 225−266, and 268−289) (*40*), and recently, residues 218−266 have been proposed to dimerize via intermolecular coiled-coil helix formation (*41*).

The results of CD measurements of the C-terminal-truncated mutants (Figure 1 and Table 1) indicate that residues 261−299 form α-helical structure whereas residues 192−260 are largely nonhelical in the lipid-free apoE4 molecule. Supporting this, the number of α-helical residues in the 10-kDa fragment derived from CD measurements (39 amino acids) corresponds to the number of amino acids in the segment spanning residues 261−299. However, comparison of the number of α-helical residues for the 10-kDa fragment (39 amino acids) and the 12-kDa fragment (53 amino acids) suggests that there is some helicity in residues 192−222 that include the hinge region. This agrees with the secondary structure prediction in which residues 203−223 form α-helical structure (*40*).

The relatively random coil-rich structure of the C-terminal domain in apoE4 proposed above is reminiscent of the situation in apoA-I that has a two-domain structure similar to that of apoE (*36*, *50*). Like apoE, apoA-I is proposed to have a distinct C-terminal segment that is responsible for oligomerization and lipid binding (*36*, *50*, *51*). Mutagenesis (*36*, *52*), electron paramagnetic resonance spectroscopy (*51*), and cross-linking/mass spectroscopy (*53*) analyses demonstrated that the C-terminal region (residues 187−243) in apoA-I has predominantly nonhelical structure in which there is a stable helical segment in the extreme C-terminus (residues 220−243). This α-helix in the C-terminus appears to function as a trigger for lipid binding accompanied by the transition of random coil to α-helix in the region including residues 187−220 (*36*, *51*), providing an energetic source for high affinity binding of apoA-I to lipids (*54*). Given the structural similarity of apoA-I and apoE (*36*), it is likely that they bind to lipid by a similar mechanism. Thus, in the case of apoE4, initial lipid binding probably occurs through α-helical segments (residues 261−299) in the C-terminal domain accompanied by an increase in α-helicity in the random coil regions of this domain which include residues 223−260. Consistent with this idea, deletion of residues 273−299 largely reduced the lipid-binding ability of apoE4 and the further deletion mutant (Δ261−299) displayed similar binding to the 22-kDa fragment (Figure 8), indicating the critical role of residues 261−299 in the lipid binding of apoE4. These findings are consistent with previous observations showing that deletion of residues 260−299 greatly diminishes the ability of the truncated apoE4 to solubilize multilamellar vesicles (*48*). In addition, the truncation to residue 260 in apoE4 markedly reduced lipoprotein association whereas that to 272 displayed identical lipoprotein distribution to the intact protein (*21*).

Gel filtration chromatography experiments revealed that the truncation of residues 273−299 or 261−299 in apoE4 gives rise to the monomeric form, consistent with previous results showing that residues 267−299 are responsible for the tetramerization of apoE in solution (*16*). Using protein engineering techniques, Fan et al. (*20*) identified five bulky hydrophobic residues in the region of residues 253−289 (Phe257, Trp264, Val269, Leu279, and Val287) that participate in hydrophobic interactions which stabilize the tetramer. Interestingly, some of these hydrophobic residues appear to be responsible for the neurotoxicity caused by the C-terminal-truncated apoE4 molecule (*31*). In addition, hydrophobic residues between amino acids 261−269 were shown to account to a large extent for the contribution of the C-terminal domain to the apoE-induced hypertriglyceridemia (*55*).

Monitoring Trp-264 fluorescence in single Trp mutants gave an interesting insight into the structural organization of the C-terminal domain in apoE. As shown in Figure 5 and Table 2, the conformational stability and cooperativity of the C-terminal domain in apoE4 is much lower than those of the 10-kDa and 12-kDa fragments. We previously demonstrated that the altered N- and C-terminal domain interaction in apoE4 (the domains are relatively closely spaced in apoE4 (*23*)) is responsible for the less organized structure in the C-terminal domain compared to apoE3 (*25*). However, the difference in stability between the C-terminal domain in full-length apoE4 and the isolated C-terminal fragments is unlikely to result from domain interaction effects because the conformational stability of the C-terminal domain in apoE3 assessed by Trp-264 fluorescence using the single Trp mutant was similar to that in apoE4 (unpublished data). Rather, it is possible that the intramolecular spatial proximity between the N- and C-terminal domains in apoE caused by weak hydrophobic interaction (*44*) affects the quaternary organization of the C-terminal domain.

The finding that residues 192−272 do not contribute to the structural stability of the C-terminal-truncated mutants (Figure 4) suggests that this region exists predominantly as a random coil structure. More directly, GdnHCl denaturation results using single Trp mutants (Figure 5 and Table 2) clearly show that the C-terminal domain in the Δ273−299 mutant forms much less organized, uncooperative structure compared with the situation in the full-length protein. However, comparison of ANS binding to the C-terminal-truncated mutants of apoE4 (Figure 7) indicates that the

Δ273−299 mutant still has a significant exposed hydrophobic site, predominantly created by residues 261−272. This exposed hydrophobic site is likely to result from intramolecular effects rather than intermolecular effects (variations in degree of self-association) because the Δ273−299 mutant exists in the monomeric state (Figure 6).

Such unique properties of the C-terminal domain in the apoE4 (Δ273−299) mutant, which comprises a less ordered, monomeric organization with a large exposed hydrophobic site, are probably relevant to its neurotoxic effects in AD brains. The C-terminal-truncated fragment of apoE4, apoE4 (Δ272−299), that is generated inside cultured neurons and in AD brains interacts with tau protein and phosphorylated neurofilaments to form the neurofibrillary tangle-like inclusions, triggering AD-like neurodegeneration (*28*, *30*). Although the major lipid-binding region of apoE (residues 244−272) is essential for this fragment to have neurotoxic effects, full-length apoE cannot interact with tau protein and phosphorylated neurofilaments (*28*). Potentially, the truncation of the C-terminal α-helix (residues 273−299) in apoE4 could activate the lipid-binding region in the C-terminal domain, with residues 261−272 being available for the binding to these molecules. For these interactions, the tertiary organization of the lipid-binding region seems to be critical because this region alone is insufficient for neurotoxicity (*31*). The lipid-binding region in the C-terminal domain of apoE4 is also involved in the binding to amyloid β (Aβ) peptide (*56*−*58*). Recently, interaction of apoE4 and Aβ peptide was proposed to form a reactive molecular intermediate capable of destabilizing membranes, causing lysosomal leakage and apoptosis (*59*, *60*). The binding of Aβ peptide to the C-terminal domain in apoE4 may cause the dissociation of tetramer into the monomeric, reactive apoE4 as seen by the C-terminal truncation.

In summary, the physicochemical characterization of the C-terminal-truncated apoE4 in this study has demonstrated that the truncation of residues 273−299 in apoE4 generated in AD brains leads to reorganization of the C-terminal domain, with a lipid-binding region being less organized and available for hydrophobic interaction. The C-terminal domain has been implicated in many pathologic functions of apoE4, including induction of neurofibrillary tangle-like inclusions in neurons (*28*, *30*) and interaction with Aβ peptide (*56*, *58*). Thus, our findings provide more molecular insight into the effects of the structural organization of the C-terminal domain in apoE4 on disease.

ACKNOWLEDGMENT

The authors thank Yoshiyuki Harada (Shimadzu Co., Kyoto, Japan) for his assistance with CD measurements.

REFERENCES

1. Mahley, R. W. (1988) Apolipoprotein E: Cholesterol transport protein with expanding role in cell biology, *Science 240*, 622−630.
2. Weisgraber, K. H. (1994) Apolipoprotein E: structure-function relationships, *Adv. Protein Chem. 45*, 249−302.
3. Mahley, R. W., and Rall, S. C., Jr. (2000) Apolipoprotein E: far more than a lipid transport protein, *Annu. Rev. Genomics Hum. Genet. 1*, 507−537.
4. Strittmatter, W. J., and Bova Hill, C. (2002) Molecular biology of apolipoprotein E, *Curr. Opin. Lipidol. 13*, 119−123.
5. Strittmatter, W. J., and Roses, A. D. (1995) Apolipoprotein E and Alzheimer disease, *Proc. Natl. Acad. Sci. U.S.A. 92*, 4725−4727.
6. Weisgraber, K. H., and Mahley, R. W. (1996) Human apolipoprotein E: the Alzheimer's disease connection, *FASEB J. 10*, 1485−1494.
7. Ashford, J. W. (2004) APOE genotype effects on Alzheimer's disease onset and epidemiology, *J. Mol. Neurosci. 23*, 157−165.
8. Huang, Y., Weisgraber, K. H., Mucke, L., and Mahley, R. W. (2004) Apolipoprotein E: diversity of cellular origins, structural and biophysical properties, and effects in Alzheimer's disease, *J. Mol. Neurosci. 23*, 189−204.
9. Strittmatter, W. J., Saunders, A. M., Schmechel, D., Pericak-Vance, M., Enghild, J., Salvesen, G. S., and Roses, A. D. (1993) Apolipoprotein E: high-avidity binding to beta-amyloid and increased frequency of type 4 allele in late-onset familial Alzheimer disease, *Proc. Natl. Acad. Sci. U.S.A. 90*, 1977−1981.
10. Holtzman, D. M., Bales, K. R., Tenkova, T., Fagan, A. M., Parsadanian, M., Sartorius, L. J., Mackey, B., Olney, J., McKeel, D., Wozniak, D., and Paul, S. M. (2000) Apolipoprotein E isoform-dependent amyloid deposition and neuritic degeneration in a mouse model of Alzheimer's disease, *Proc. Natl. Acad. Sci. U.S.A. 97*, 2892−2897.
11. Teasdale, G. M., Nicoll, J. A., Murray, G., and Fiddes, M. (1997) Association of apolipoprotein E polymorphism with outcome after head injury, *Lancet 350*, 1069−1071.
12. Roses, A. D. (1998) Apolipoprotein E and Alzheimer's disease. The tip of the susceptibility iceberg, *Ann. N.Y. Acad. Sci. 855*, 738−743.
13. Saito, H., Lund-Katz, S., and Phillips, M. C. (2004) Contributions of domain structure and lipid interaction to the functionality of exchangeable human apolipoproteins, *Prog. Lipid Res. 43*, 350−380.
14. Wilson, C., Wardell, M. R., Weisgraber, K. H., Mahley, R. W., and Agard, D. A. (1991) Three-dimensional structure of the LDL receptor-binding domain of human apolipoprotein E, *Science 252*, 1817−1822.
15. Narayanaswami, V., and Ryan, R. O. (2000) Molecular basis of exchangeable apolipoprotein function, *Biochim. Biophys. Acta 1483*, 15−36.
16. Westerlund, J. A., and Weisgraber, K. H. (1993) Discrete carboxyl-terminal segments of apolipoprotein E mediate lipoprotein association and protein oligomerization, *J. Biol. Chem. 268*, 15745−15750.
17. Segrest, J. P., Garber, D. W., Brouillette, C. G., Harvey, S. C., and Anantharamaiah, G. M. (1994) The amphipathic α-helix: a multifunctional structural motif in plasma apolipoproteins, *Adv. Protein Chem. 45*, 303−369.
18. Saito, H., Dhanasekaran, P., Baldwin, F., Weisgraber, K. H., Lund-Katz, S., and Phillips, M. C. (2001) Lipid binding-induced conformational change in human apolipoprotein E. Evidence for two lipid-bound states on spherical particles, *J. Biol. Chem. 276*, 40949−40954.
19. Perugini, M. A., Schuck, P., and Howlett, G. J. (2000) Self-association of human apolipoprotein E3 and E4 in the presence and absence of phospholipid, *J. Biol. Chem. 275*, 36758−36765.
20. Fan, D., Li, Q., Korando, L., Jerome, W. G., and Wang, J. (2004) A monomeric human apolipoprotein E carboxyl-terminal domain, *Biochemistry 43*, 5055−5064.
21. Dong, L. M., Wilson, C., Wardell, M. R., Simmons, T., Mahley, R. W., Weisgraber, K. H., and Agard, D. A. (1994) Human apolipoprotein E. Role of arginine 61 in mediating the lipoprotein preferences of the E3 and E4 isoforms, *J. Biol. Chem. 269*, 22358−22365.
22. Dong, L. M., and Weisgraber, K. H. (1996) Human apolipoprotein E4 domain interaction. Arginine 61 and glutamic acid 255 interact to direct the preference for very low-density lipoproteins, *J. Biol. Chem. 271*, 19053−19057.
23. Hatters, D. M., Budamagunta, M. S., Voss, J. C., and Weisgraber, K. H. (2005) Modulation of apolipoprotein E structure by domain interaction: differences in lipid-bound and lipid-free forms, *J. Biol. Chem. 280*, 34288−34295.
24. Drury, J., and Narayanaswami, V. (2005) Examination of lipid-bound conformation of apolipoprotein E4 by pyrene excimer fluorescence, *J. Biol. Chem. 280*, 14605−14610.
25. Saito, H., Dhanasekaran, P., Baldwin, F., Weisgraber, K. H., Phillips, M. C., and Lund-Katz, S. (2003) Effects of polymorphism on the lipid interaction of human apolipoprotein E, *J. Biol. Chem. 278*, 40723−40729.

26. Xu, Q., Brecht, W. J., Weisgraber, K. H., Mahley, R. W., and Huang, Y. (2004) Apolipoprotein E4 domain interaction occurs in living neuronal cells as determined by fluorescence resonance energy transfer, *J. Biol. Chem. 279*, 25511−25516.
27. Raffai, R. L., Dong, L. M., Farese, R. V., Jr., and Weisgraber, K. H. (2001) Introduction of human apolipoprotein E4 "domain interaction" into mouse apolipoprotein E, *Proc. Natl. Acad. Sci. U.S.A. 98*, 11587−11591.
28. Huang, Y., Liu, X. Q., Wyss-Coray, T., Brecht, W. J., Sanan, D. A., and Mahley, R. W. (2001) Apolipoprotein E fragments present in Alzheimer's disease brains induce neurofibrillary tangle-like intracellular inclusions in neurons, *Proc. Natl. Acad. Sci. U.S.A. 98*, 8838−8843.
29. Brecht, W. J., Harris, F. M., Chang, S., Tesseur, I., Yu, G. Q., Xu, Q., Dee Fish, J., Wyss-Coray, T., Buttini, M., Mucke, L., Mahley, R. W., and Huang, Y. (2004) Neuron-specific apolipoprotein e4 proteolysis is associated with increased tau phosphorylation in brains of transgenic mice, *J. Neurosci. 24*, 2527−2534.
30. Harris, F. M., Brecht, W. J., Xu, Q., Tesseur, I., Kekonius, L., Wyss-Coray, T., Fish, J. D., Masliah, E., Hopkins, P. C., Scearce-Levie, K., Weisgraber, K. H., Mucke, L., Mahley, R. W., and Huang, Y. (2003) Carboxyl-terminal-truncated apolipoprotein E4 causes Alzheimer's disease-like neurodegeneration and behavioral deficits in transgenic mice, *Proc. Natl. Acad. Sci. U.S.A. 100*, 10966−10971.
31. Chang, S., Ma, T. R., Miranda, R. D., Balestra, M. E., Mahley, R. W., and Huang, Y. (2005) Lipid- and receptor-binding regions of apolipoprotein E4 fragments act in concert to cause mitochondrial dysfunction and neurotoxicity, *Proc. Natl. Acad. Sci. U.S.A. 102*, 18694−18699.
32. Morrisett, J. D., David, J. S., Pownall, H. J., and Gotto, A. M., Jr. (1973) Interaction of an apolipoprotein (apoLP-alanine) with phosphatidylcholine, *Biochemistry 12*, 1290−1299.
33. Acharya, P., Segall, M. L., Zaiou, M., Morrow, J., Weisgraber, K. H., Phillips, M. C., Lund-Katz, S., and Snow, J. (2002) Comparison of the stabilities and unfolding pathways of human apolipoprotein E isoforms by differential scanning calorimetry and circular dichroism, *Biochim. Biophys. Acta 1584*, 9−19.
34. Sparks, D. L., Lund-Katz, S., and Phillips, M. C. (1992) The charge and structural stability of apolipoprotein A-I in discoidal and spherical recombinant high-density lipoprotein particles, *J. Biol. Chem. 267*, 25839−25847.
35. Eftink, M. R. (2000) Use of fluorescence spectroscopy as thermodynamics tool, *Methods Enzymol. 323*, 459−473.
36. Saito, H., Dhanasekaran, P., Nguyen, D., Holvoet, P., Lund-Katz, S., and Phillips, M. C. (2003) Domain structure and lipid interaction in human apolipoproteins A-I and E, a general model, *J. Biol. Chem. 278*, 23227−23232.
37. Lund-Katz, S., Weisgraber, K. H., Mahley, R. W., and Phillips, M. C. (1993) Conformation of apolipoprotein E in lipoproteins, *J. Biol. Chem. 268*, 23008−23015.
38. Lund-Katz, S., Zaiou, M., Wehrli, S., Dhanasekaran, P., Baldwin, F., Weisgraber, K. H., and Phillips, M. C. (2000) Effects of lipid interaction on the lysine microenvironments in apolipoprotein E, *J. Biol. Chem. 275*, 34459−34464.
39. Liu, L., Bortnick, A. E., Nickel, M., Dhanasekaran, P., Subbaiah, P. V., Lund-Katz, S., Rothblat, G. H., and Phillips, M. C. (2003) Effects of apolipoprotein A-I on ATP-binding cassette transporter A1-mediated efflux of macrophage phospholipid and cholesterol: formation of nascent high-density lipoprotein particles, *J. Biol. Chem. 278*, 42976−42984.
40. Segrest, J. P., Jones, M. K., De Loof, H., Brouillette, C. G., Venkatachalapathi, Y. V., and Anantharamaiah, G. M. (1992) The amphipathic helix in the exchangeable apolipoproteins: a review of secondary structure and function, *J. Lipid Res. 33*, 141−166.
41. Choy, N., Raussens, V., and Narayanaswami, V. (2003) Intermolecular coiled-coil formation in human apolipoprotein E C-terminal domain, *J. Mol. Biol. 334*, 527−539.
42. Morrow, J. A., Segall, M. L., Lund-Katz, S., Phillips, M. C., Knapp, M., Rupp, B., and Weisgraber, K. H. (2000) Differences in stability among the human apolipoprotein E isoforms determined by the amino-terminal domain, *Biochemistry 39*, 11657−11666.
43. Morrow, J. A., Hatters, D. M., Lu, B., Hochtl, P., Oberg, K. A., Rupp, B., and Weisgraber, K. H. (2002) Apolipoprotein E4 forms a molten globule. A potential basis for its association with disease, *J. Biol. Chem. 277*, 50380−50385.
44. Narayanaswami, V., Szeto, S. S., and Ryan, R. O. (2001) Lipid association-induced N- and C-terminal domain reorganization in human apolipoprotein E3, *J. Biol. Chem. 276*, 37853−37860.
45. Aggerbeck, L. P., Wetterau, J. R., Weisgraber, K. H., Wu, C. S., and Lindgren, F. T. (1988) Human apolipoprotein E3 in aqueous solution. II. Properties of the amino- and carboxyl-terminal domains, *J. Biol. Chem. 263*, 6249−6258.
46. Chou, C. Y., Lin, Y. L., Huang, Y. C., Sheu, S. Y., Lin, T. H., Tsay, H. J., Chang, G. G., and Shiao, M. S. (2005) Structural variation in human apolipoprotein E3 and E4: secondary structure, tertiary structure, and size distribution, *Biophys. J. 88*, 455−466.
47. Weers, P. M., Narayanaswami, V., Choy, N., Luty, R., Hicks, L., Kay, C. M., and Ryan, R. O. (2003) Lipid binding ability of human apolipoprotein E N-terminal domain isoforms: correlation with protein stability?, *Biophys. Chem. 100*, 481−492.
48. Li, X., Kypreos, K., Zanni, E. E., and Zannis, V. (2003) Domains of apoE required for binding to apoE receptor 2 and to phospholipids: implications for the functions of apoE in the brain, *Biochemistry 42*, 10406−10417.
49. Wilson, C., Mau, T., Weisgraber, K. H., Wardell, M. R., Mahley, R. W., and Agard, D. A. (1994) Salt bridge relay triggers defective LDL receptor binding by a mutant apolipoprotein, *Structure 2*, 713−718.
50. Davidson, W. S., Hazlett, T., Mantulin, W. W., and Jonas, A. (1996) The role of apolipoprotein AI domains in lipid binding, *Proc. Natl. Acad. Sci. U.S.A. 93*, 13605−13610.
51. Oda, M. N., Forte, T. M., Ryan, R. O., and Voss, J. C. (2003) The C-terminal domain of apolipoprotein A−I contains a lipid-sensitive conformational trigger, *Nat. Struct. Biol. 10*, 455−460.
52. Gorshkova, I. N., Liadaki, K., Gursky, O., Atkinson, D., and Zannis, V. I. (2000) Probing the lipid-free structure and stability of apolipoprotein A-I by mutation, *Biochemistry 39*, 15910−15919.
53. Silva, R. A., Hilliard, G. M., Fang, J., Macha, S., and Davidson, W. S. (2005) A three-dimensional molecular model of lipid-free apolipoprotein A-I determined by cross-linking/mass spectrometry and sequence threading, *Biochemistry 44*, 2759−2769.
54. Saito, H., Dhanasekaran, P., Nguyen, D., Deridder, E., Holvoet, P., Lund-Katz, S., and Phillips, M. C. (2004) α-Helix formation is required for high affinity binding of human apolipoprotein A-I to lipids, *J. Biol. Chem. 279*, 20974−20981.
55. Kypreos, K. E., van Dijk, K. W., Havekes, L. M., and Zannis, V. I. (2005) Generation of a recombinant apolipoprotein E variant with improved biological functions: hydrophobic residues (LEU-261, TRP-264, PHE-265, LEU-268, VAL-269) of apoE can account for the apoE-induced hypertriglyceridemia, *J. Biol. Chem. 280*, 6276−6284.
56. Pillot, T., Goethals, M., Najib, J., Labeur, C., Lins, L., Chambaz, J., Brasseur, R., Vandekerckhove, J., and Rosseneu, M. (1999) β-Amyloid peptide interacts specifically with the carboxy-terminal domain of human apolipoprotein E: relevance to Alzheimer's disease, *J. Neurochem. 72*, 230−237.
57. Phu, M. J., Hawbecker, S. K., and Narayanaswami, V. (2005) Fluorescence resonance energy transfer analysis of apolipoprotein E C-terminal domain and amyloid β peptide (1−42) interaction, *J. Neurosci. Res. 80*, 877−886.
58. Strittmatter, W. J., Weisgraber, K. H., Huang, D. Y., Dong, L. M., Salvesen, G. S., Pericak-Vance, M., Schmechel, D., Saunders, A. M., Goldgaber, D., and Roses, A. D. (1993) Binding of human apolipoprotein E to synthetic amyloid beta peptide: isoform-specific effects and implications for late-onset Alzheimer disease, *Proc. Natl. Acad. Sci. U.S.A. 90*, 8098−8102.
59. Ji, Z. S., Miranda, R. D., Newhouse, Y. M., Weisgraber, K. H., Huang, Y., and Mahley, R. W. (2002) Apolipoprotein E4 potentiates amyloid β peptide-induced lysosomal leakage and apoptosis in neuronal cells, *J. Biol. Chem. 277*, 21821−21828.
60. Ji, Z. S., Mullendorff, K., Cheng, I. H., Miranda, R. D., Huang, Y., and Mahley, R. W. (2006) Reactivity of Apolipoprotein E4 and Amyloid β Peptide: Lysosomal Stability and Neurodegeneration, *J. Biol. Chem. 281*, 2683−2692.

BI060023B